Aalborg Universitet

AALBORG UNIVERSITY
DENMARK

Application-Driven Data Acquisition for Condition Monitoring of Power Semiconductors in Traction Inverter Applications

Wei, Xing; Jin, Long; Yao, Bo; Peng, Yingzhou; Wang, Huai

Published in:
IEEE Transactions on Transportation Electrification

DOI (link to publication from Publisher):
10.1109/TTE.2023.3339848

Creative Commons License
CC BY 4.0

Publication date:
2024

Document Version
Accepted author manuscript, peer reviewed version

Link to publication from Aalborg University

Citation for published version (APA):
Wei, X., Jin, L., Yao, B., Peng, Y., & Wang, H. (2024). Application-Driven Data Acquisition for Condition Monitoring of Power Semiconductors in Traction Inverter Applications. *IEEE Transactions on Transportation Electrification*, *10*(3), 6812-6824. https://doi.org/10.1109/TTE.2023.3339848

General rights
Copyright and moral rights for the publications made accessible in the public portal are retained by the authors and/or other copyright owners and it is a condition of accessing publications that users recognise and abide by the legal requirements associated with these rights.

- Users may download and print one copy of any publication from the public portal for the purpose of private study or research.
- You may not further distribute the material or use it for any profit-making activity or commercial gain
- You may freely distribute the URL identifying the publication in the public portal -

Take down policy
If you believe that this document breaches copyright please contact us at vbn@aub.aau.dk providing details, and we will remove access to the work immediately and investigate your claim.

Downloaded from vbn.aau.dk on: February 07, 2025

Application-Driven Data Acquisition for Condition Monitoring of Power Semiconductors in Traction Inverter Applications

Xing Wei, *Student Member, IEEE*, Long Jin, Bo Yao, *Student Member, IEEE*, Yingzhou Peng, *Member, IEEE*, Huai Wang, *Senior Member, IEEE*

***Abstract*—Condition monitoring has proven to be an effective means of enhancing the reliability of power semiconductors. This paper proposes an innovative and practical data acquisition scheme that can serve various condition monitoring purposes for power semiconductors in traction inverter applications. It is achieved through the DC-link discharging operation mode of the traction inverter after the system is shut down, minimizing the new risks introduced by condition monitoring into system operation, which is critical to the safety of traction applications. Moreover, due to the extremely low dynamics in the discharging operation mode, the sampling requirements for the health indicators and operating conditions of power semiconductors are greatly reduced, and the measurement disturbances from parasitic parameters are eliminated. The proposed method is promising for electric vehicle (EV) applications as the required operation condition is an inherently programmed and frequent mode. Compared to conventional online data acquisition schemes, it outperforms in complexity, accuracy, safety, and practicality. The proof-of-concept experiments based on a three-phase inverter prototype verify the effectiveness of the proposed method.**

***Index terms*—** Condition monitoring, traction inverter, electric vehicle, power semiconductor, data acquisition.

I. Introduction

POWER semiconductors play a crucial role in power converter systems, contributing to cost, size, and failure rate on a considerable scale [1–3]. To achieve reliable field operation, numerous health indicators for power semiconductors have been proposed, such as on-state saturation voltage [4, 5], pre/threshold voltage [6, 7], Miller platform voltage [8], gate peak current [9], and switching times [10, 11], etc. These indicators are widely utilized for condition monitoring purposes [12, 13], including degradation assessment and junction temperature estimation for power semiconductors, to enable proactive maintenance, thermal management, and operation optimization.

Due to the inherent characteristics of semiconductors, the health indicators of power semiconductors depend on both their degradation states and operating conditions [14], the latter of which include conduction current and junction temperature. As a result, relying solely on health indicator information is not sufficient for either condition monitoring purpose. In junction temperature estimation applications, modeling the relationship between junction temperature and health indicators is a prerequisite and critical step [15–18], where health indicators for specific operating conditions and synchronized junction temperature information are needed. Similarly, for the degradation assessment of power semiconductors [19, 20], synchronized information on the health indicators and their associated operating conditions is required to calibrate the effect of operating conditions on the health indicators.

The above data requirements indicate that to achieve the condition monitoring of power semiconductors, the health indicators and their associated operating conditions have to be measured synchronously and accurately, as shown in Fig. 1. In addition, in existing condition monitoring schemes, data acquisition is commonly performed online during the normal operation of the power converter [12, 13], where a high sampling rate is essential due to the high dynamics. In practice, however, these demanding data acquisition requirements are generally difficult to fulfill and face the following challenges:

1) Challenges in existing measurement conditions

For most power electronic converters, their existing measurement systems are designed for control purposes, where the converter signals are typically measured asynchronously at a sampling frequency of up to the switching frequency and without the need for high-precision sensors. These non-ideal data acquisition conditions mean that there could be errors in the measured health indicators and operating conditions, which can seriously affect the accuracy of condition monitoring, especially for junction temperature estimation applications as the health indicators of power semiconductors generally have a low sensitivity to the junction temperature, e.g. mV / °C of on-state voltage [4, 5] and ns / °C of switching times [10, 11]. It has been reported in [17] that due to the dependence of the health

Manuscript received xx; revised xx; accepted xx. This work was supported by the National Natural Science Foundation of China, under grant 52207203. (Corresponding author: Long Jin, Bo Yao.).

X. Wei, B. Yao, and H. Wang are with the Department of Energy, Aalborg University, Aalborg, Denmark (email: xwe@energy.aau.dk, ybo@energy.aau.dk, hwa@energy.aau.dk).

X. Wei and L. Jin are with the School of Electrical Engineering, Southeast University, Jiangsu, China (e-mail: xwe@energy.aau.dk, jinlong@seu.edu.cn).

Y. Peng is with the College of Electrical and Information Engineering, Hunan University, Hunan, China (e-mail:yzpeng@hnu.edu.cn).

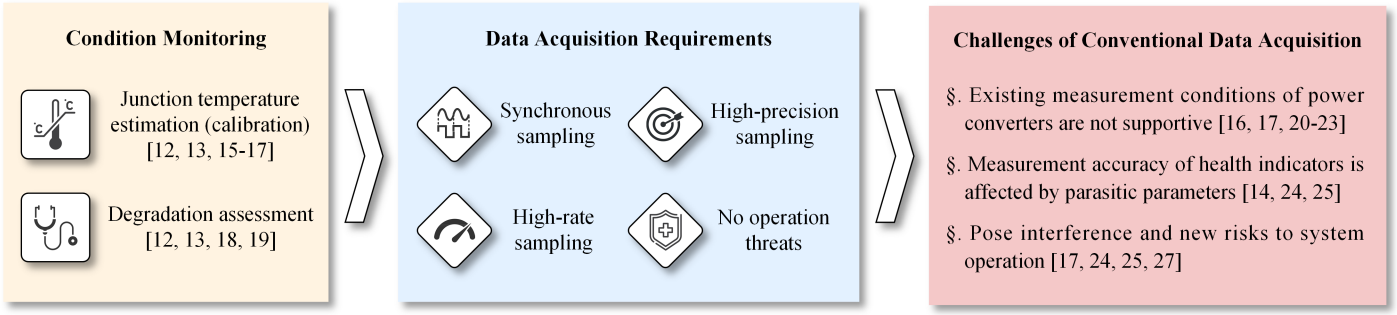

Fig. 1. Data acquisition requirements and challenges for condition monitoring of power semiconductors.

indicators of power semiconductors on the conduction current, a small current variation of 0.5 % can cause a temperature difference of nearly 4 °C. In [18], due to the absence of synchronized current sampling, the on-state voltage of power semiconductors used for junction temperature calibration is measured over a small current range instead of at a certain value, and the resulting fluctuations in the measured on-state voltage cause an error up to ± 6 °C in the calibration results.

It is worth noting that some operating conditions of power semiconductors are inherently difficult to obtain, such as junction temperature. Due to the external packaging for protection and electrical insulation, the direct measurement of junction temperature based on optical properties [21] or physical contact [22] has restrictions in practical applications. Some model-based methods [23, 24] are proposed to estimate the junction temperature indirectly by leveraging the power loss and thermal models of power semiconductors, but there can be considerable errors in the calculated power losses and thermal impedance, resulting in inaccurate estimation.

Overall, the above challenges in terms of measurement conditions indicate that the existing measurement systems of power converters are generally inadequate for condition monitoring purposes and need to be upgraded or augmented with additional hardware measurement, which is, however, costly and impractical for most field applications.

2) Challenges in parasitic parameters and system security

In practice, the online data acquisition adopted by conventional condition monitoring schemes is not necessary for some application purposes, such as degradation assessment, because the degradation of power semiconductors is typically a long-term process. In addition, online data acquisition can be disturbed by the parasitic parameters of power semiconductors and pose a threat to the security of power converters.

During the normal operation of power converters, the alternating load current can induce voltages in the parasitic inductances distributed in the direct copper bond (DCB) layer, bond wires, and terminals of power semiconductors [14], and these induced voltages are not constant due to the variable slope of current. As a result, the voltages measured across the terminals of power semiconductors can deviate and lead to measurement errors in the related health indicators, e.g., on-state saturation voltage and Miller platform voltage. Particularly in high-power applications, where the load current changes dramatically and the inductive parasitic elements of power semiconductors are considerable, the resulting errors in the measured health indicators can be significant. In [25] and [26], the on-state voltage of power semiconductors in an operating wind turbine converter and traction inverter is measured at a constant current level, and the deviation in the measured on-state voltage caused by parasitic inductances reaches 7.5 % and 6.1 %, respectively. Considering the low temperature sensitivity of the on-state voltage and the degradation-induced increase in on-state voltage is typically 5 % to 20 % [27], such a considerable measurement deviation could be unacceptable.

Safety is paramount for power converters, and therefore the risks posed by condition monitoring to the system operation should be minimized. However, online data acquisition can occupy significant storage resources during the normal operation of the power converter, which may affect the data processing and storage performance of the system. More importantly, online data acquisition means that the hardware measurements dedicated to condition monitoring are also activated during normal operation, which can introduce additional reliability issues to the system operation. In [28], a junction temperature calibration method for the power semiconductors in wind turbine applications is disclosed, where three months of data on health indicators and operating conditions, covering the entire converter power range are recorded online. The long-term measurement and extensive data logging seriously threaten the safe operation of power converters.

In conclusion, the aforementioned challenges in terms of existing measurement conditions, parasitic parameters, and system security serve as major obstacles, hindering the implementation of condition monitoring for power semiconductors in practice. In this paper, a novel condition monitoring-oriented data acquisition scheme is proposed for power semiconductors in traction inverter applications. It is performed during the discharge of the inverter DC-link capacitor after the system shutdown, which is a natural and frequent activity in traction applications such as electric vehicles. The collected data on health indicators and operating conditions can be utilized for various condition monitoring purposes of power semiconductors, including degradation assessment and junction temperature calibration. Compared to conventional online data acquisition methods, the proposed scheme shows that:

1) the measurement requirements for health indicators and operating conditions of power semiconductors are greatly reduced;
2) the measurement of health indicators is independent of the parasitic parameters of power semiconductors;
3) the interference and new risks posed by condition monitoring to system operation are minimized;
4) the operating conditions of power semiconductors are controllable, convenient for various monitoring requirements.

The rest of this article is organized as follows: Section II introduces the DC-link discharging operation mode of the traction inverter through the motor stator windings. Section III presents the principles of the discharge profile-based data acquisition for condition monitoring purposes. Section IV gives the proof-of-concept of the proposed method based on experimental testing, followed by the conclusion in Section V.

II. DC-link Discharge of Traction Inverter through Motor Stator Windings

The electrical configuration of the traction inverter is depicted in Fig. 2, consisting of a DC-link capacitor, power semiconductor devices, and a controller. Its front end is typically connected to a battery pack or rectifier via circuit breakers, and the back-end electric machine (EM) can be either an AC induction machine or an AC permanent magnet type [29]. To achieve high operating power, the power semiconductor devices in the current traction inverter are commonly insulated gate bipolar transistors (IGBTs), which are expected to be replaced by silicon carbide (SiC) and gallium nitride (GaN) devices in the future to further reduce power loss and system size [3]. Depending on the baseplate design of the power device, a direct-liquid or forced-air cooling system is generally equipped to regulate the device operating temperature.

After normal operation, the gate drivers of the power semiconductor devices in the traction inverter are first blocked, causing a rapid decrease in the three-phase traction current i_{a}, i_{b}, and i_{c}. For safety reasons, when the electronic control unit (ECU) detects that the traction currents and motor speed have dropped to zero, the circuit breakers in Fig. 2 are opened to isolate the traction inverter, and subsequently, a pair of discharge commands, $i_{\mathrm{d\_ref}}$ and $i_{\mathrm{q\_ref}}$, in the rotor flux reference frame is issued to discharge the DC-link capacitor [30]. With the existing current control and modulation strategy (typically space vector pulse width modulation), the DC-link capacitor is discharged through the power devices and the back-end motor stator windings according to the rotor electrical angle θ_{e} as well as the discharge current references $i_{\mathrm{d\_ref}}$ and $i_{\mathrm{q\_ref}}$. The rotor electrical angle θ_{e} is fixed in a DC-link discharge, which is random and determined by the shutdown profile in traction inverters with synchronous motors, while it can be set arbitrarily in traction inverters with asynchronous motors. The d-axis current reference $i_{\mathrm{d\_ref}}$ can be any value within the inverter rating as long as it meets the discharge time requirements (typically less than 1 s), but the q-axis current reference $i_{\mathrm{q\_ref}}$ must be set to null to avoid torque generation.

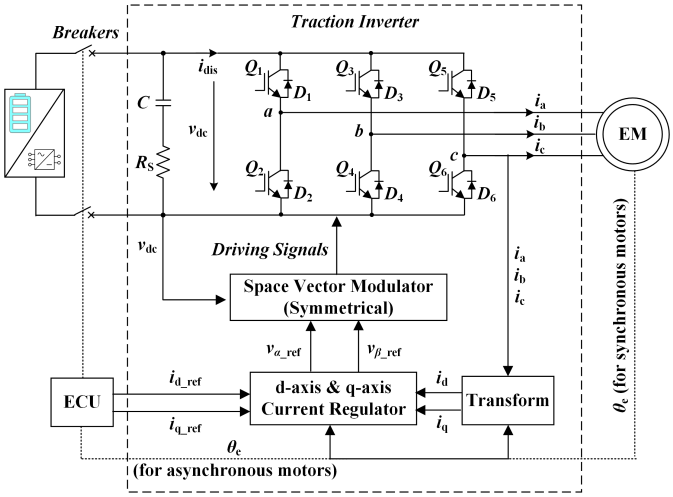

Fig. 2. Electrical configuration of the traction inverter. C and R_{S} are the capacitance and equivalent series resistance (ESR) of the DC-link capacitor, ECU is the electronic control unit, EM is the load electric motor, Q_1 – Q_6 and D_1 – D_6 represent the IGBT devices and free-wheeling diodes in the power semiconductor module, respectively.

TABLE I
Specifications of the Traction Inverter System Built in the Simulation Platform PLECS

DC-link Film Capacitor	
Capacitance C	645 μF @ 100 Hz
ESR R_{S}	4 mΩ @ 100 Hz
IGBT Power Module	
Product	Infineon FS820R08A6P2B [30]
Cooling form	Direct-liquid cooling
Switching frequency	10 kHz
Electric Motor	
Type	Permanent-magnet synchronous motor
Stator winding resistance	5.7 mΩ
d-axis winding inductance	120 μH
q-axis winding inductance	320 μH
Pole pairs	4
Permanent magnet flux linkage	63 * 10^{-3} Wb

A directly liquid-cooled traction inverter system is built in the simulation platform PLECS with the specifications given in Table I. To calculate the junction temperature of the IGBT devices, the simulation model is configured with the power loss model of the devices and the Foster thermal model [31] between the device junction and the coolant, both of which are available from the power module datasheet [32]. Fig. 3 gives the simulation waveforms of the traction inverter after the system shutdown, where a DC-link discharge profile with the initial DC-link voltage of 300 V, d-axis current reference

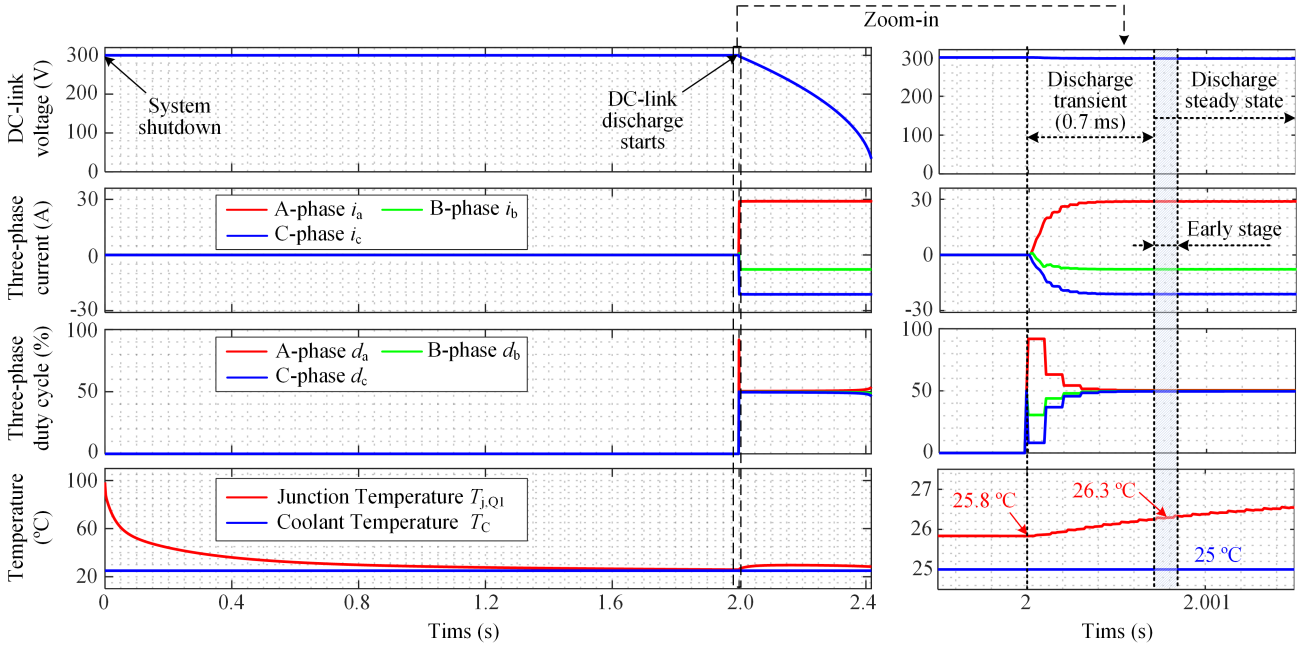

Fig. 3. Simulation waveforms of a directly liquid-cooled traction inverter after the system shutdown, including a DC-link discharge profile with the initial DC-clink voltage V_{C0} of 300 V, d-axis current reference i_{d_ref} of 30 A, rotor electrical angle θ_e of $\pi/12$, and coolant temperature T_C of 25 °C. d_a, d_b, and d_c stand for the duty cycles of the upper switches in each phase leg, and $T_{j,Q1}$ is the junction temperature of the IGBT Q_1 in Fig. 2.

i_{d_ref} of 30 A, rotor electrical angle θ_e of $\pi/12$, and coolant temperature T_C of 25 °C is included. It can be seen that the DC-link capacitor of the traction inverter starts to discharge after the system is shut down for 2 s, followed by a gradual decrease in the DC-link voltage. Due to the constant rotor electrical angle, the three-phase stator current has fixed polarity in the discharge and reaches a steady state after a short transient, where the steady-state current value is independently determined by the current reference i_{d_ref} and the rotor electrical angle θe, e.g., i_a=i_{d_ref}*cos(θe). According to the current characteristics, the discharge process is divided into two stages: discharge transient and discharge steady state, as labeled in the zoom-in in Fig. 3. The duty cycles of the three-phase upper switches are all around 50 % within the steady-state interval, and the discharge is concluded when the DC-link voltage falls below a safety voltage (e.g., 36 V).

III. Discharge Profile-based Data Acquisition for Condition Monitoring Purposes

In this paper, the IGBT power device with wire bonding packaging and direct liquid-cooled PinFin baseplate, as shown in Fig. 4, is taken as the case study to illustrate the methodology. In principle, the proposed data acquisition scheme is also applicable to traction applications employing other power semiconductor types and cooling forms.

A. Acquisition of Operating Conditions

It is known that the operating conditions of power semiconductors, including conduction current and junction temperature, are necessary information to achieve their condition monitoring. The conduction current of a power semiconductor device is

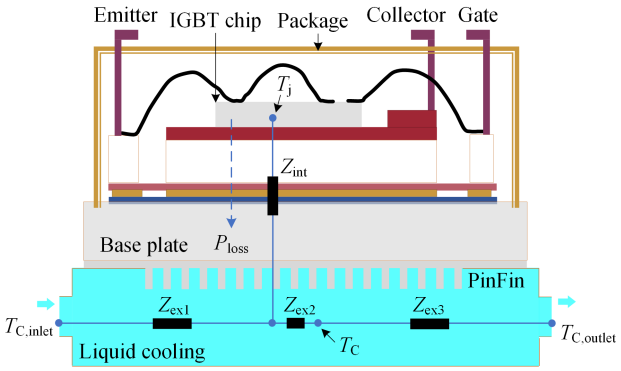

Fig. 4. Structure and heat dissipation route of an IGBT device with wire bonding packaging and direct liquid-cooled PinFin baseplate. P_{loss} is the power loss generated by the device chip, T_j is the junction temperature, T_C is the reference coolant temperature, $T_{C,inlet}$ and $T_{C,outlet}$ are the temperatures at the inlet and outlet of the liquid-cooling system, Z_{int} and $Z_{ex,1/2/3}$ represent the internal and external thermal impedance for the power device, respectively.

determined by the corresponding phase current and is equal to it in the on-state, but the device junction temperature is generally difficult to obtain in practice due to the external packaging. Taking the IGBT Q_1 in Fig. 2 as an example, its junction temperature $T_{j,Q1}$ can be expressed as a function of the power loss, transient thermal impedance, and a reference temperature (e.g., coolant temperature T_C) based on Foster thermal network [31], as given by

$$T_{j,Q1} = \begin{bmatrix} R_{jC,11}\left(1-e^{-t/\tau_{11}}\right) \\ R_{jC,21}\left(1-e^{-t/\tau_{21}}\right) \\ \cdots \\ R_{jC,61}\left(1-e^{-t/\tau_{61}}\right) \end{bmatrix}^T \times \begin{bmatrix} P_{loss,1} \\ P_{loss,2} \\ \cdots \\ P_{loss,6} \end{bmatrix} + T_C \quad (1)$$

where $R_{\mathrm{jC},11}$ and τ_{11} are the self-thermal resistance and self-thermal time constant of the IGBT Q_1 from its junction to a reference coolant point, $R_{\mathrm{jC},21}$ - $R_{\mathrm{jC},61}$ and τ_{21} - τ_{61} are the coupled thermal resistance and couple thermal time constants between the IGBT Q_1 and the other five power devices, respectively. $P_{\mathrm{loss},1}$ - $P_{\mathrm{loss},6}$ are the averaged power losses generated by the six power devices in the traction inverter over one fundamental cycle.

After the traction inverter is shut down, the power losses $P_{\mathrm{loss},1}$ - $P_{\mathrm{loss},6}$ in (1) drops to zero immediately with the three-phase traction current. Since the self- and coupled thermal time constants of direct liquid-cooled power devices are typically small, the device junction temperature can be reduced to the coolant temperature in a short term, as shown in Fig. 3, where the coolant temperature is 25 °C and the junction temperature $T_{\mathrm{j,Q1}}$ of the IGBT Q_1 decreases from 100 °C to 25.8 °C within 2 s after shutdown. It implies that if the interval between the system shutdown and the subsequent discharge event is long enough, the device junction temperature in the DC-link discharge is independent of the inverter mission profile before shutdown. Further, the zoom-in in Fig. 3 gives the waveforms at the beginning of the DC-link discharge, from which it can be seen that the duration of the discharge transient process is extremely short, about 0.7 ms, which means that the first term on the right side of (1) during the discharge transient can be low enough to lead to a negligible difference between T_{j} and T_{C}, compared to T_{C}. As a result, it can be assumed that the device junction temperature at the early stage of the discharge steady state is equal to the coolant temperature before discharge. In Fig. 3, the junction temperature $T_{\mathrm{j,Q1}}$ of the IGBT Q_1 at the early stage of the discharge steady state is 1.3 °C only higher than the coolant temperature of 25 °C.

In field applications, it is worth noting that the reference coolant temperature T_{C} is typically calculated by averaging the inlet temperature $T_{\mathrm{C,inlet}}$ and the outlet temperature $T_{\mathrm{C,outlet}}$ of the liquid cooling system [27]. This implies that the point corresponding to the reference coolant temperature T_{C} may not be located centrally below the device chip of interest, and the thermal network between the device junction and the reference coolant temperature point can be regarded as consisting of an internal thermal impedance Z_{int} and an external thermal impedance Z_{ex2}, as illustrated in Fig. 4. Once the liquid cooling conditions change, the external thermal impedance Z_{ex2} will also be changed, and as a result, the device junction temperature T_{j} may require a longer time after the system shutdown to decrease to the reference coolant temperature T_{C}. Generally, the impact of this external thermal impedance change is minor because the power module is typically mounted at the center of the liquid cooling system, but if it cannot be ignored in some field applications, there are two solutions: (1) extend the time interval between the system shutdown and the subsequent DC-link discharge; (2) utilize the NTC temperature as the reference temperature to approximate the junction temperature since the heat dissipation route between the device junction and the NTC is mainly provided by the internal thermal network of the power module [33], which is mainly determined by the module material and structure and is barely affected by the external environment conditions. Similarly, in traction applications with forced-air cooling, the case and NTC temperatures of the power module are preferred to be used as the reference temperatures because the heat dissipation routes are also predominantly inside the power module, as verified in Section IV. B.

Overall, if the health indicators of power semiconductors are measured within the early stage of the discharge steady state, the associated operating conditions including conduction current and junction temperature can be obtained from the corresponding phase current and a reference temperature, respectively. In addition, it can be known from Fig. 3 that the three-phase traction current remains constant in the discharge steady state, where the current fluctuations caused by the equivalent inductance of the motor stator windings are negligible. It implies the sampling requirements for traction currents are greatly reduced, i.e., there is no need for synchronous sampling with health indicators as well as high sampling rates.

B. Acquisition of Health Indicators

It is important to note that to minimize the error caused by using a reference temperature to approximate the device junction temperature, the health indicators should be measured as early as possible during the discharge steady state as a lower $R_{\mathrm{jC}}(1\text{-}e^{-t/\tau})$ in (1) can be obtained. Moreover, the change in the device junction temperature within the early stage of the discharge steady state is negligible due to the extremely short duration. Combined with the constant traction current, it can be considered that the health indicators of power semiconductors within the early stage of the discharge steady state are under the same operating conditions, and consequently, the sampling requirements for health indicators are also significantly reduced. Particularly, for static health indicators of power semiconductors, such as on-state saturation voltage, since the duty cycle of the power device is maintained around 50 % during the discharge steady state, as shown in Fig. 3, a large amount of health indicator data at the same operating conditions is available from the early stage interval. A recommended acquisition approach for health indicators and their associated operating conditions is to sample at the switching frequency during the initial several consecutive switching periods of the discharge steady state, and then average or median the collected data. The averaging or median filtering can effectively reduce the errors caused by noises and measurements, as well as the requirements for sensor accuracy.

In addition to reducing sampling requirements, the low dynamics of the DC-link discharging operation mode can also significantly eliminate the impact of parasitic parameters on the measurement of health indicators. Fig. 5 gives the equivalent circuit of a power semiconductor device with bond wires as the interconnections [26]. The voltages V_{CE} measured across the collector and power emitter terminals and V_{GE} measured across the gate and Kelvin emitter terminals with the power device in the on-state are given in (2), where i_{C} is the collector current, i_{g}

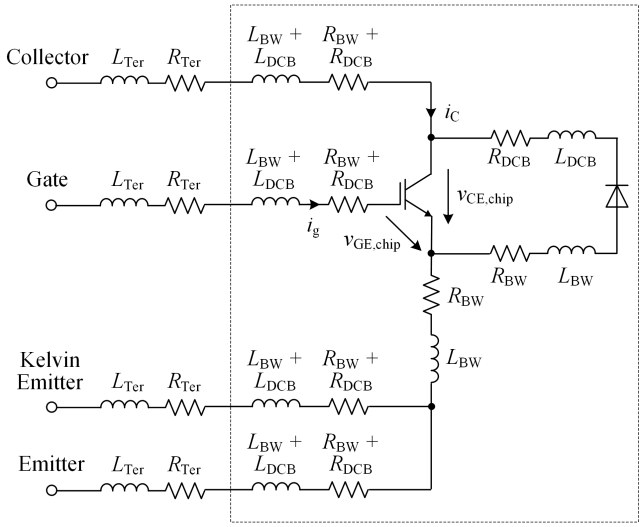

Fig. 5. Equivalent circuit of a power semiconductor device with bond wires as interconnections [26].

is the gate current, $L_{\rm Ter/BW/DCB}$ and $R_{\rm Ter/BW/DCB}$ represent the parasitic inductance and resistance distributed inside the connection terminals, bond wires, and direct copper bond (DCB) layers of the power device, respectively. The parasitic resistances enable these terminal voltages with sensitivity to the package-related degradation (e.g., bond-wire fatigue) of power devices and can therefore be used for degradation assessment, but the parasitic inductances can seriously affect the accuracy of the voltage measurement. During the normal operation of the traction inverter, the derivative of the collector current $di_{\rm C}/dt$ in (2) is not constant due to the alternating traction current and can be either positive or negative even at the same operating conditions, which will lead to a considerable deviation in the measured terminal voltages, resulting in unacceptable errors in the health indicators. In contrast, the derivative term $di_{\rm C}/dt$ tends to zero in the DC-link discharge steady state due to the constant traction current, and thus the measurement of health indicators is independent of the parasitic inductances.

$$\begin{cases} V_{\rm CE} = V_{\rm CE,chip} + i_{\rm C}R_{\rm tot} + L_{\rm tot}\frac{di_{\rm C}}{dt} \\ V_{\rm GE} = V_{\rm GE,chip} + i_{\rm g}R_{\rm tot} + L_{\rm tot}\frac{di_{\rm g}}{dt} + i_{\rm C}R_{\rm BW} + L_{\rm BW}\frac{di_{\rm C}}{dt} \\ R_{\rm tot} = 2R_{\rm Ter} + 3R_{\rm BW} + 2R_{\rm DCB} \\ L_{\rm tot} = 2L_{\rm Ter} + 3L_{\rm BW} + 2L_{\rm DCB} \end{cases} \tag{2}$$

In summary, the proposed discharge profile-based data acquisition scheme allows an accurate measurement of the health indicators and operating conditions of power semiconductors under reduced sampling conditions. Moreover, as the DC-link discharge occurs after the traction inverter is shut down, the proposed method does not occupy the storage resources during normal operation or introduce additional reliability issues, minimizing the interference and new risks posed by condition monitoring to the system operation. Furthermore, the operating conditions of the DC-link discharge, especially the steady-state value of the three-phase traction current, are controllable in field applications. For traction inverters with asynchronous motors, the steady-state currents can be controlled by both the current reference $i_{\rm d\_ref}$ and the rotor electrical angle $\theta_{\rm e}$. While in traction applications with synchronous motors, the steady-state currents can still be controlled by $i_{\rm d\_ref}$ although $\theta_{\rm e}$ is random. The controllability of the operating conditions means that the data requirements of various condition monitoring purposes can be satisfied. For example, in the junction temperature calibration applications for power semiconductors, several pairs of synchronized health indicators and junction temperature information for specific operating conditions are required, which can be conveniently obtained by controlling a few DC-link discharge events, as verified by a case study in Section IV. D. It is worth stating that the initial DC-link voltage is an important operation variable for the DC-link discharging operation mode that affects the discharge duration, which, however, has no effect on the proposed scheme because the health indicators and operating conditions of power semiconductors are acquired at the early stage of the discharge steady state and before the discharge, respectively.

C. Practical Implementation Considerations

The proposed data acquisition method can be implemented in traction inverters employing any type of power semiconductor, cooling system, and load electric motor, and can also be extended to other inverter applications with motor loads, such as aerospace drives, provided that the following two prerequisites are fulfilled: 1) the application has the shutdown events and the inverter DC-link can be discharged through the motor stator windings; 2) the application has a measurable reference temperature (e.g., coolant temperature, module case temperature, or NTC temperature) to which the device junction temperature can drop within a short time after the system is shut down. For the second prerequisite, the interval between system shutdown and DC-link discharge can be extended appropriately if necessary to ensure that the junction temperature converges with the reference temperature before the discharge, and it is worth noting that this prerequisite is naturally fulfilled in some applications. In electric vehicle applications, for example, the three-phase traction current drops to zero immediately after the vehicle is parked, and the circuit breakers between the battery and the traction inverter only open after the vehicle is locked. This implies that the time interval between the system shutdown and the DC-link discharge is determined by driver behavior and is bound to be longer than the small thermal time constant between the device junction and the reference temperature.

In practical implementation, for the existing traction inverters, the deployment of the proposed data acquisition scheme could be software- and hardware-invasive. Although for safety reasons most traction inverters have a DC-link discharge after system shutdown, it is implemented with an auxiliary electric network consisting of switches and resistors in some applications. In this case, the DC-link discharging operation mode through the motor stator windings should be added to the control software and the signal acquisition system needs to

remain active after the system shutdown. In addition, since most of the existing traction inverters do not have the condition monitoring function originally, there could be a lack of measurements for health indicators and some operating conditions. Therefore, some additional hardware (e.g., sensors) may be required and the measured signals have to be transferred to the existing acquisition system of the traction inverter to ensure data synchronization. For the future new-generation traction inverters, these required software controls and hardware measurements can be pre-deployed and integrated during the design phase. It is recommended to reserve redundancy in data processing capabilities for future functionality expansion, as condition monitoring applications like degradation assessment typically require further data processing to achieve more advanced functions, e.g., remaining useful lifetime prediction. It is worth pointing out that although condition monitoring is a novel and promising application that can effectively improve the reliability of traction inverters in practice, it can also increase product cost due to the demand for additional hardware measurements and software resources. As a result, there is a trade-off between the cost and the requirements for product reliability and innovation.

IV. Experimental Verification

A. Experimental Setup

To verify the feasibility of the proposed method, a three-phase inverter prototype is built, as shown in Fig. 6 (a), along with its hardware realization and specifications are given in Fig. 6 (b) and Table II, respectively. The DC-link of the inverter prototype is designed with a film capacitor of ELECTRONICON$^{\mathrm{TM}}$ PK16 [34], and the power semiconductor devices adopt the IGBT module of Infineon FS35R12KT3 [35], which is mounted on an aluminum heatsink with a cooling fan and a temperature-controlled heating system. A PLECS RT box is used as the controller to implement the closed-loop current control with symmetrical space vector modulation, and the switching frequency of the power devices is set at 10 kHz. Constrained by the power capacity and space of the laboratory, the stator windings of the back-end electric motor are simulated by a three-phase RL load. In the DC-link discharging operation mode, since the motor rotor is clamped resulting in a zero back electromotive force, it could be reasonable to equate the load motor with the RL loads.

The proposed data acquisition scheme is applicable to various health indicators of power semiconductors, and the on-state saturation voltage is selected here as the case study for methodology validation, which is one of the most widely investigated indicators. The IGBT Q_1 in Fig. 6 (a) is taken as the device under test (DUT), and during DC-link discharge, the collector-emitter voltage of the DUT consists of the DC-link voltage and its on-state voltage, where the high amplitude of the DC-link voltage implies that a voltage sensor with a wide measurement range is required. To exclude this requirement, the measurement circuit proposed in [36] is connected to the collector and emitter terminals of the DUT, as shown in Fig. 6 (a), which is

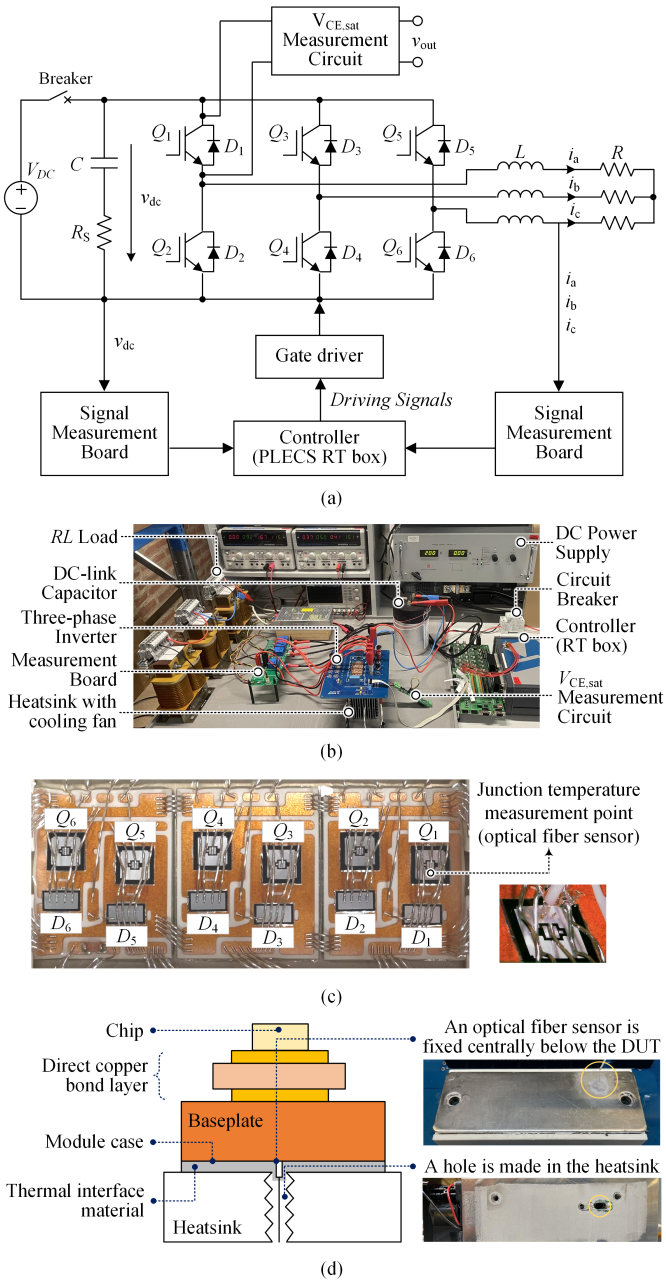

Fig. 6. A three-phase inverter prototype for verification. (a) Inverter topology. The on-state voltage measurement circuit [36] is connected to the collector and emitter of the IGBT Q_1 to extract its on-state voltage information. (b) Hardware realization with an IGBT module of Infineon FS35R12KT3 [35]. (c) Layout of the IGBT module and measurement point of an optical fiber temperature sensor [37] on the DUT. (4) Measurement of the module case temperature with an optical fiber temperature sensor [37].

capable of clamping the high-amplitude DC-link voltage in the collector-emitter voltage to a low reference voltage, and retaining the low-amplitude on-state voltage components in its output v_{out}. For error analysis, the plastic case of the IGBT module is removed, and an optical fiber temperature sensor (OTG-F type from OPsens) [37] is placed at the center of the chip surface of the DUT to measure its junction temperature directly, as shown in Fig. 6 (c). The response time and resolution of the optical sensor are 5 ms and 0.05 °C, respectively.

TABLE II
SPECIFICATIONS OF THE THREE-PHASE INVERTER PROTOTYPE

DC-link Film Capacitor	
Product	Electronicon™ PK16 [32]
Capacitance C	656.7 µF @ 100 Hz
ESR R_S	1.06 mΩ @ 100 Hz
IGBT Power Module	
Product	Infineon FS35R12KT3 [33]
Rated current	35 A
Maximum operating voltage	1200 V
Cooling form	Forced-air cooling
Switching frequency	10 kHz
RL load	
Resistance R	50 mΩ @ 100 Hz
Inductance L	7.2 mH @ 100 Hz
Signal measurement boards	
Measured signals	v_{dc}, i_a, i_b, i_c, d_a, d_b, d_c, $T_{j,Q1}$, T_{Case}, T_{ntc}, v_{out}

v_{dc} is the DC-link voltage; i_a, i_b, and i_c are the three-phase load current; d_a, d_b, and d_c are the duty cycles of the three-phase upper switches; $T_{j,Q1}$ is the junction temperature of the IGBT Q_1; T_{Case} is the module case temperature; T_{NTC} is the module NTC temperature; v_{out} is the output of the on-state voltage measurement circuit.

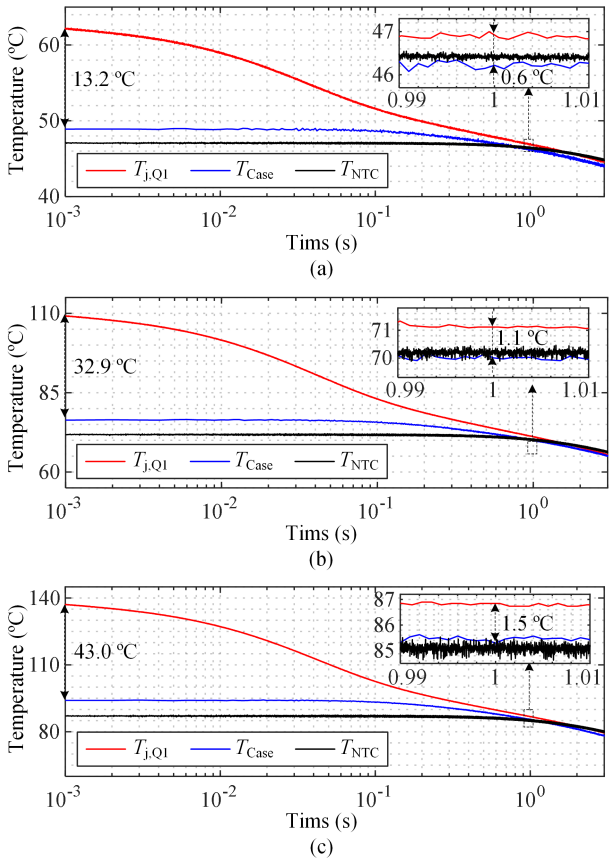

Fig. 7. Decrease curves of the junction temperature $T_{j,Q1}$ of the DUT, the module case temperature T_{Case}, and the module NTC temperature T_{NTC} after the inverter prototype is shut down for an initial difference between $T_{j,Q1}$ and T_{Case} of △ 13.2 °C, △ 32.9 °C, and △ 43.0 °C, respectively.

B. Inverter Shutdown and DC-link Discharge Profiles

Since the power module FS35R12KT3 employs a smooth copper baseplate, the module case temperature T_{Case} is taken as the reference temperature in this case study. The measurement of the case temperature follows the guidelines in AQG 324 [27], as shown in Fig. 6 (d), where a hole is made in the aluminum heatsink and an optical fiber temperature sensor (OTG-F type from OPsens) [37] is fixed centrally below the DUT. From the module datasheet [35], it can be known that the thermal time constant between the device junction and the module case is about 1 s, which is similar to the thermal time constant between the device junction and the coolant of direct liquid-cooled power modules, e.g., Infineon FS820R08A6P2B [32]. This implies that the following experimental validation of the module case temperature is also informative for using the coolant temperatures as the reference temperatures in direct liquid-cooled applications.

To verify the feasibility of approximating the device junction temperature with the module case temperature, the inverter prototype is first operated under different mission profiles to achieve a temperature difference of △ 13.2 °C, △ 32.9 °C, and △ 43.0 °C between the junction temperature $T_{j,Q1}$ of the DUT and the module case temperature T_{Case}, respectively, and Fig. 7 gives the drop curves of these two temperatures after the inverter is shut down. It can be seen that due to the small thermal time constant, the junction temperature $T_{j,Q1}$ can be reduced to the case temperature T_{Case} within 1 s, and is independent of the initial temperature difference. This indicates that if the DC-link discharge is conducted after the inverter shutdown for 1 s, the device junction temperature during the discharge is independent of the previous mission profile. It is worth noting that in some field applications, the module case temperature could be difficult to obtain as there is no hole in the heatsink for mounting a temperature sensor. In this case, the module NTC temperature T_{NTC} can potentially be used as the reference temperature. The drops curves of the NTC temperature T_{NTC} after the inverter shutdown are also given in Fig. 7, which is measured with a signal converter (WAS6 TTA from Weidmuller) [38] and it can be seen the DUT junction temperature $T_{j,Q1}$ can also converge with the NTC temperature T_{NTC} after 1 s of the system shutdown. Additionally, it can be noted from Fig. 7 that the time for the DUT junction temperature $T_{j,Q1}$ to drop to the case and NTC temperatures is independent of the initial junction temperature, which indirectly indicates that the internal thermal impedance of the power module is independent of the external environmental conditions, e.g., temperature.

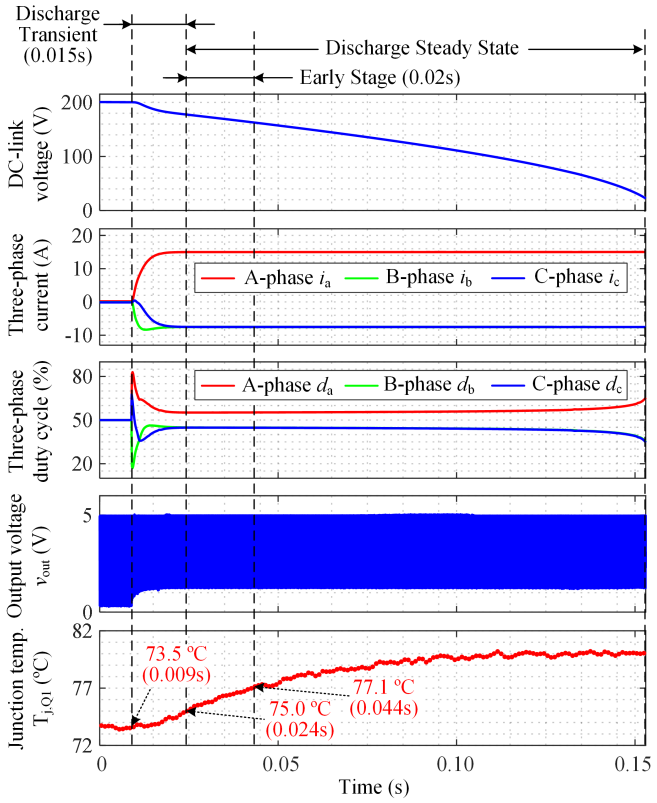

Fig. 8. An experimental discharge profile of the inverter prototype with the initial DC-link voltage V_{C0} of 200 V, d-axis current reference i_{d_ref} of 15 A, rotor electrical angle θ_e of 0π, and case temperature T_{Case} of 73.5 °C.

Fig. 8 gives an experimental discharge profile of the inverter prototype with the initial DC-link voltage V_{C0} of 200 V, d-axis current reference i_{d_ref} of 15 A, rotor electrical angle θ_e of 0π, and module case temperature T_{Case} of 73.5 °C, where both i_{d_ref} and θ_e are set in the controller, i.e., the PLECS RT box. The electrical signals in Fig. 8 are all sampled at 100 kHz and the junction temperature of the DUT is sampled at 1 kHz. It can be seen that the DC-link discharge starts at 0.009 s, followed by a gradual decrease in the DC-link voltage. The three-phase load current reaches the steady state at about 0.024 s after a short transient, and the steady-state current is precisely controlled at the target value by the current reference i_{d_ref} and the rotor electrical angle θ_e. The duty cycles of the three-phase upper switches are maintained around 50 % during the discharge steady state, and eventually, the discharge is concluded after the DC-link voltage falls below 20 V. The output v_{out} of the on-state voltage measurement circuit during the discharge is also given in Fig. 8, where the DC-link voltage in the collector-emitter voltage of the DUT is clamped at a reference voltage of 5 V, and the on-state voltage information of the DUT is retained.

In Fig. 8, the junction temperature $T_{j,Q1}$ of the DUT has stabilized at the case temperature T_{Case} of 73.5 °C before the DC-link discharge. As the duration of the transient process in the discharge is extremely short, about 0.015 s in Fig. 8, the junction temperature $T_{j,Q1}$ rises from the case temperature T_{Case} to 75 °C only after the transient. This indicates that the module case temperature is a valid reference temperature in this case study to approximate the junction temperature of the DUT at the early stage of the discharge steady state. Considering a relatively poor case, if the health indicators of power semiconductors are measured within the early stage of the discharge steady state of up to 0.02 s labeled in Fig. 8, the maximum error caused by using the case temperature before discharge to approximate the device junction temperature is 3.6 °C only, which is acceptable for most field applications.

TABLE III
SAMPLING CONDITIONS FOR THE OUTPUT OF THE ON-STATE VOLTAGE MEASUREMENT CIRCUIT

Case	Sampling rate	Sampling form	Additional sampling error
1	10 kHz	Random	/
2	1 kHz	Random	/
3	100 Hz	Random	/
4	100 Hz	Random	± 5% Random error

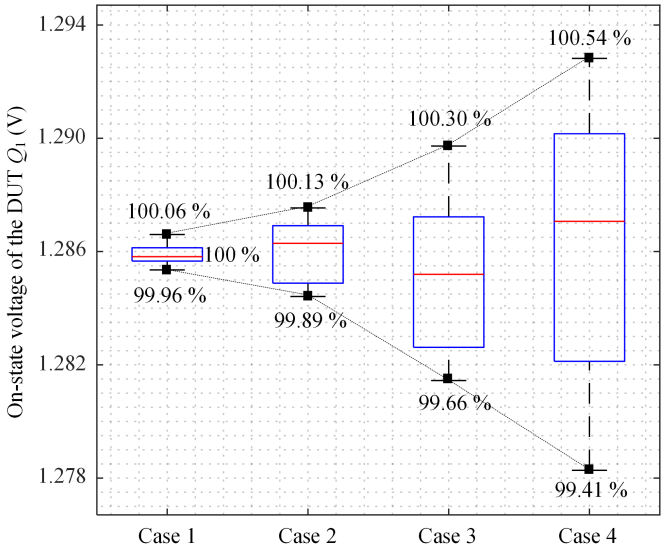

Fig. 9. Median results of the DUT on-state voltage measured over the early stage of the discharge steady state with the different sampling conditions in Table III, where each case contains 20 discharge profiles with the initial DC-link voltage V_{C0} of 200 V, d-axis current reference i_{d_ref} of 15 A, rotor electrical angle θ_e of 0π, and case temperature T_{Case} of 73.5 °C.

C. Discharge Profile-based Data Acquisition

The constancy of the load currents in the discharge steady state shown in Fig. 8 demonstrates their easy accessibility and that high-rate and synchronized current sampling with health indicators is not required. Additionally, it can be known from Fig. 8 that the change in the junction temperature $T_{j,Q1}$ of the DUT within the labeled early stage is 2.1 °C only, and the duty cycle d_a of the DUT is maintained at 55 %. Therefore, it can be considered that there is a large amount of on-state voltage data for the DUT under the same operating condition is available in this early stage interval, resulting in much lower sampling requirements for the on-state voltage.

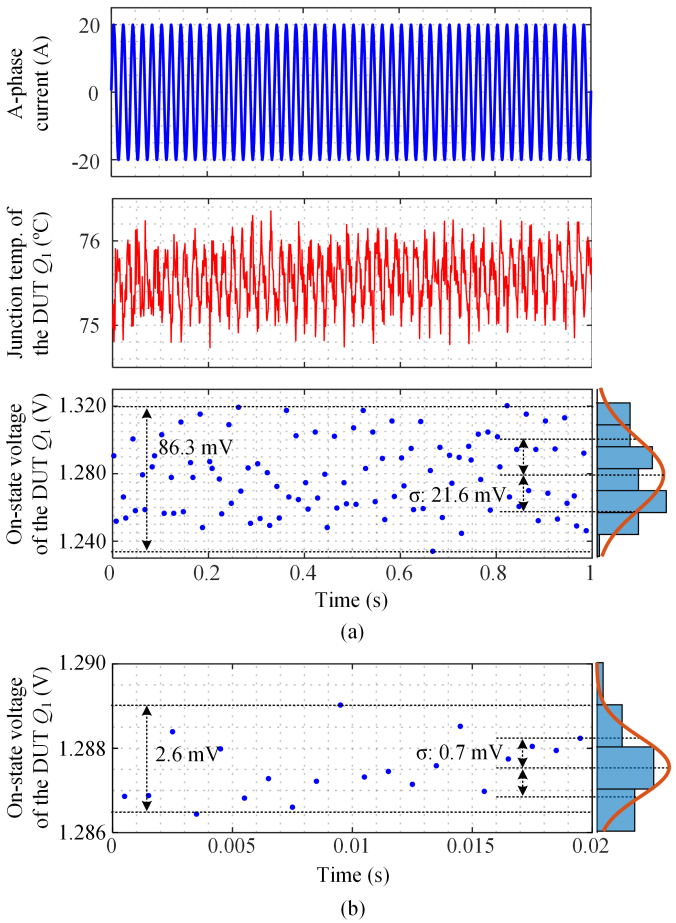

Fig. 10. On-state voltage of the DUT with a collector current of 15 A measured during (a) a period of operation of the inverter prototype with a peak load current of 20 A, a fundamental frequency of 50 Hz, and a DUT junction temperature of 75.5 °C; (b) the early steady state of a DC-link discharge with the d-axis current reference of 15 A, rotor electrical angle of 0π, and module case temperature of 75 °C. σ denotes the standard deviation of the data cluster.

To verify this conjecture, the output v_{out} of the on-state voltage measurement circuit during the DC-link discharge is sampled with different sampling conditions, as given in Table III, where the DC-link discharge with the initial DC-link voltage V_{C0} of 200 V, d-axis current reference $i_{\text{d\_ref}}$ of 15 A, rotor electrical angle θ_{e} of 0π, and module case temperature T_{Case} of 73.5 °C is performed 20 times in each case. The maximum sampling rate of 10 kHz is chosen in consideration of the fact that the signal sampling rate in real traction inverters is typically not higher than the switching frequency, and the sampling form of random means that the sampling occurs randomly within the corresponding sampling period. An additional random error of up to $\pm$ 5 % is introduced into the discharge profiles for Case 4 to simulate a more severe sampling condition, e.g., sensor with a lower accuracy, analog to digital converter (ADC) with a lower bits, and greater system noise. Fig. 9 gives the median result of the DUT on-state voltage collected over the early stage of the discharge steady state for 20 discharge tests in each case, where the early stage of the discharge steady state is defined as in Fig. 8 within the 0.02 s interval after 0.015s from the start of the DC-link discharge. It can be seen that if the median of the box plot for Case 1 is taken as the base value, the absolute acquisition deviation for the on-state voltage of the DUT is within 0.4 % in Cases 1 to 3, and is less than 0.6 % even in Case 4 where the sampling frequency is 100 times lower than the switching frequency and there is an additional $\pm$ 5 % random error, validating the low sampling requirements.

To illustrate the impact of parasitic parameters on the acquisition of health indicators, the three-phase inverter prototype is scheduled to operate at a peak load current of 20 A and a fundamental frequency of 50 Hz. Fig. 10 (a) gives the operating waveforms when the junction temperature of the DUT reaches a steady state of 75.5 °C, where the on-state voltage of the DUT is measured at the A-phase current of 15 A. It can be seen that the deviation in the on-state voltage measured for the same collector current and junction temperature conditions reaches 86.3 mV, with a standard deviation σ of 21.6 mV. By testing the I-V characteristics of the DUT at different temperature levels, it is known that the sensitivity of the on-state voltage of the DUT to its junction temperature at the collector current of 15 A is 0.6 mV/°C only. Therefore, this measurement deviation is mainly caused by parasitic inductances and the contribution of junction temperature fluctuation is negligible. To verify the effectiveness of the low dynamics of the DC-link discharging operation mode in suppressing the effects of parasitic inductance, the discharge test of the inverter prototype is conducted under the similar operating conditions with the module case temperature T_{Case} of 75 °C, d-axis current reference $i_{\text{d\_ref}}$ of 15 A, and rotor electrical angle θ_{e} of 0π. The on-state voltage of the DUT within the early stage (initial 0.02 s interval) of the discharge steady state is given in Fig. 10 (b), where the on-state voltage is sampled at 1 kHz. It can be seen that the deviation in the measured on-state voltage is 2.6 mV only and the standard deviation σ is reduced by 31 times compared to that in normal operation. It is worth stating that the average values of the on-state voltage of the DUT in Fig. 10 (a) and (b) are 1.2785 V and 1.2875 V, respectively, with a deviation of 9 mV although these on-state voltage data are collected under similar operating conditions. This average discrepancy is mainly caused by the measurement errors and the voltages induced on the parasitic inductors of the DUT that cannot be well averaging filtered.

D. Case Study of Junction Temperature Calibration

Junction temperature estimation is an important application of health indicators for power semiconductors, with the prerequisite that the relationship between health indicators and junction temperature has been calibrated for a specific operating condition [15, 16]. By taking the DUT Q_1 as an example, its junction temperature $T_{\text{j,Q1}}$ can be estimated indirectly by its on-state voltage $V_{\text{CE,sat1}}(I_{\text{C}})$ at a specific collector current I_{C} due to the linear relationship given in (3), and the coefficients a and b must be parameterized in advanced before estimation.

$$T_{\text{j,Q1}} = aV_{\text{CE,sat1}}\left(I_{\text{C}}\right) + b \tag{3}$$

Based on the proposed data acquisition method, this calibration routine can be conveniently accomplished in a short

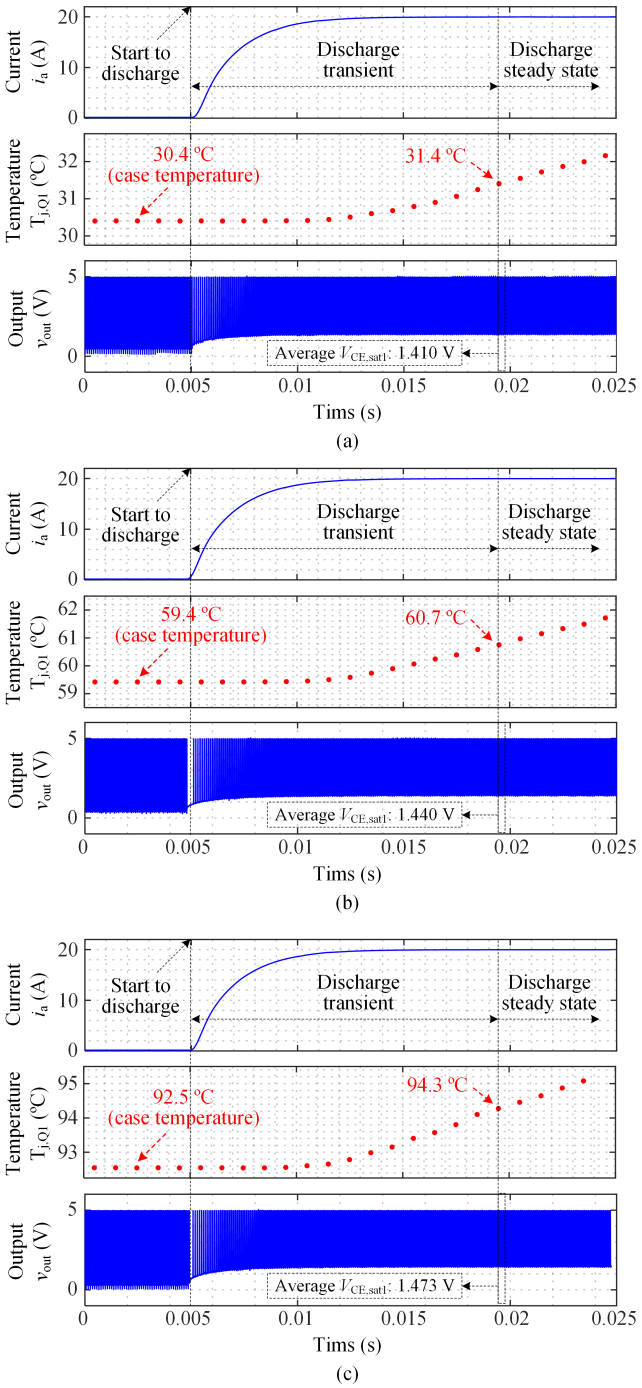

Fig. 11. DC-link discharge profiles of the inverter prototype with the current reference $i_{\mathrm{d\_ref}}$ of 20 A, rotor electrical angle θ_{e} of 0π, and initial module case temperature T_{Case} of (a) 30.4 °C, (b) 59.4 °C, and (c) 92.5 °C, respectively, where the discharges all start at 0.05 s and reach a steady state 0.0195 s. v_{out} is the output of the on-state voltage measurement circuit.

term with several discharge events. Since the module case temperature before discharge has been proven to be a valid reference temperature for approximating the device junction temperature at the early stage of the discharge steady state, the parameterization of the coefficients a and b in (3) can be achieved by fitting several pairs of the case temperature before

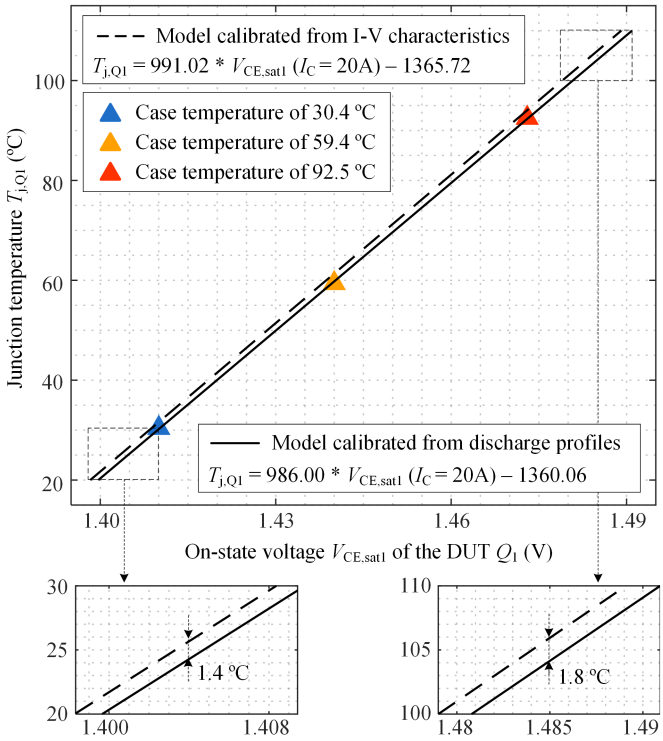

Fig. 12. Junction temperature estimation model of the DUT Q_1 calibrated with the proposed data acquisition method. The off-line calibration result obtained by I-V characteristic tests is given for comparison.

discharge and on-state voltage within the early steady-state interval obtained from discharge profiles at different temperature levels but with the same steady-state A-phase current of I_{C}.

To calibrate the DUT Q_1 at a collector current I_{C} of 20 A, the DC-link discharge of the inverter prototype is carried out with the current reference $i_{\mathrm{d\_ref}}$ of 20 A, rotor electrical angle θ_{e} of 0π, and module case temperature T_{Case} of 30.4 °C, 59.4 °C, and 92.5 °C, respectively. The current reference $i_{\mathrm{d\_ref}}$ and rotor angle θ_{e} are set to control the calibration current level, and at least one of them is controllable in field applications. The different case temperatures T_{Case} are achieved by adjusting the heatsink temperature, which is not necessary in practice and the different temperature levels are existing due to the complex mission profiles before the system shutdown. Fig. 11 gives the discharge profiles for each case, where the DC-link discharges all start at 0.005 s and reach a steady state at 0.0195s. It can be seen that the junction temperature $T_{\mathrm{j,Q1}}$ of the DUT Q_1 is initially stabilized at the case temperature T_{Case} and then gradually increases with the DC-link discharge. The increase in the junction temperature $T_{\mathrm{j,Q1}}$ during the discharge transient increases with the case temperature level due to higher power losses, but the maximum rise is 1.8 °C only occurs in Fig. 11 (c). This indicates that if the on-state voltage used for calibration is measured at the early stage of the discharge steady state, the calibration using the module case temperature instead of the device junction temperature causes an error of a few degrees only. To guarantee calibration accuracy and eliminate measurement errors, the on-state voltage of the DUT Q_1 in the

initial five switching periods of the discharge steady state is sampled at 10 kHz, and the average value of the sampled data is used for calibration.

The recorded module case temperature T_{Case} and average on-state voltage $V_{\mathrm{CE,sat1}}$ for each case are marked with triangles in Fig. 12, and the junction temperature estimation model calibrated by fitting these data points is plotted with a solid line. For comparison purposes, the I-V characteristics of the DUT Q_1 are tested for off-line calibration and the calibration result is plotted by a dashed line in Fig. 12. It can be seen that due to the error caused by calibrating with module case temperature, the junction temperature estimation model calibrated from discharge profiles is on the low side, and the deviation increases with the junction temperature. This is because the difference between the module case temperature before discharge and the junction temperature at the early stage of the discharge steady state is greater in the DC-link discharge with higher temperature levels. However, in general, the model calibrated from discharge profiles exhibits high similarity to the off-line calibration result with a maximum deviation limited to 2 °C, which validates that a calibration with comparable accuracy to the off-line calibration can be achieved with the proposed data acquisition method. Ultimately, the junction temperature $T_{\mathrm{j,Q1}}$ of the DUT Q_1 can be estimated in real-time by substituting the measured $V_{\mathrm{CE,sat1}}$ into the calibrated model.

V. Conclusions

This paper proposes an innovative data acquisition scheme for the health indicators and operating conditions of power semiconductors in traction inverter applications, aiming to facilitate the implementation of their condition monitoring applications in practice. It is achieved through the DC-link discharging operation mode of the traction inverter after the system shutdown and is expected to overcome the challenges of existing condition monitoring schemes in terms of measurement complexity, accuracy, and safety. The experimental validation is conducted with a three-phase inverter prototype and the results show that: 1) the operating conditions of power semiconductors, including conduction current and junction temperature, are easily accessible and the synchronous and high-rate sampling is no longer required; 2) the health indicators of power semiconductors can be accurately acquired even under reduced measurement conditions, e.g., at a sampling frequency 100 times lower than the switching frequency and with considerable measurement errors; 3) the measurement deviation of health indicators caused by parasitic parameters can be reduced by 31 times in this case study; 4) with the proposed acquisition method, the junction temperature calibration of power semiconductors can be conveniently accomplished with three discharge events only, and a comparable accuracy with the off-line calibration can be achieved. As a next step, the authors will implement the proposed data acquisition scheme in specific condition monitoring applications of power semiconductors, including junction temperature calibration, degradation assessment, and remaining useful lifetime prediction, to further validate its feasibility and effectiveness.

References

[1] J. Falck, C. Felgemacher, A. Rojko, M. Liserre, and P. Zacharias, "Reliability of power electronic systems: an industry perspective," *IEEE Ind. Electron. Mag.*, vol. 12, no. 2, pp. 24–35, Jun. 2018.

[2] H. Wang, M. Liserre, and F. Blaabjerg, "Toward reliable power electronics: challenges, design tools, and opportunities," *IEEE Ind. Electron. Mag.*, vol. 7, no. 2, pp. 17–26, Jun. 2013.

[3] F. Blaabjerg, H. Wang, I. Vernica, B. Liu, and P. Davari, "Reliability of power electronic systems for EV/HEV applications," *Proc. IEEE*, vol. 109, no. 6, pp. 1060–1076, Jun. 2021.

[4] J. Chen, E. Deng, L. Xie, X. Ying, and Y. Huang, "Investigations on averaging mechanisms of virtual junction temperature determined by Vce(T) method for igbts," *IEEE Trans. Electron Devices*, vol. 67, no. 3, pp. 1106–1112, Mar. 2020.

[5] X. Wei, B. Yao, Y. Peng, and H. Wang, "Junction temperature estimation for igbt modules through knee voltage," in *2022 International Power Electronics Conference (IPEC-Himeji 2022- ECCE Asia)*. Himeji, Japan: IEEE, May 2022, pp. 461–465.

[6] R. Mandeya, C. Chen, V. Pickert, and R. T. Naayagi, "Prethreshold voltage as a low-component count temperature sensitive electrical parameter without self-heating," *IEEE Trans. Power Electron.*, vol. 33, no. 4, pp. 2787–2791, Apr. 2018.

[7] G. Zeng, H. Cao, W. Chen, and J. Lutz, "Difference in device temperature determination using p-n-junction forward voltage and gate threshold voltage," *IEEE Trans. Power Electron.*, vol. 34, no. 3, pp. 2781–2793, Mar. 2019.

[8] X. Ye, C. Chen, Y. Wang, G. Zhai, and G. J. Vachtsevanos, "Online condition monitoring of power mosfet gate oxide degradation based on miller platform voltage," *IEEE Trans. Power Electron.*, vol. 32, no. 6, pp. 4776–4784, Jun. 2017.

[9] N. Baker, S. Munk-Nielsen, F. Iannuzzo, and M. Liserre, "Igbt junction temperature measurement via peak gate current," *IEEE Trans. Power Electron.*, vol. 31, no. 5, pp. 3784–3793, May 2016.

[10] F. Yang, S. Pu, C. Xu, and B. Akin, "Turn-on delay based real-time junction temperature measurement for sic mosfets with aging compensation," *IEEE Trans. Power Electron.*, vol. 36, no. 2, pp. 1280–1294, Feb. 2021.

[11] H. Luo, Y. Chen, P. Sun, W. Li, and X. He, "Junction temperature extraction approach with turn-off delay time for high-voltage high-power igbt modules," *IEEE Trans. Power Electron.*, pp. 1–1, 2015.

[12] Y. Avenas, L. Dupont, N. Baker, H. Zara, and F. Barruel, "Condition monitoring: a decade of proposed techniques," *IEEE Ind. Electron. Mag.*, vol. 9, no. 4, pp. 22–36, Dec. 2015.

[13] S. Yang, D. Xiang, A. Bryant, P. Mawby, L. Ran, and P. Tavner, "Condition monitoring for device reliability in power electronic converters: a review," *IEEE Trans. Power Electron.*, vol. 25, no. 11, pp. 2734–2752, Nov. 2010.

[14] B. J. Baliga, *Fundamentals of power semiconductor devices*. Raleigh, North Carolina, USA: Springer, 2008.

[15] Y. Avenas, L. Dupont, and Z. Khatir, "Temperature measurement of power semiconductor devices by thermo-sensitive electrical parameters—a review," *IEEE Trans. Power Electron.*, vol. 27, no. 6, pp. 3081–3092, Jun. 2012.

[16] X. Wei, B. Yao, Y. Peng, and H. Wang, "An on-line calibration method for tsep-based junction temperature estimation in ev traction inverter applications," in *2023 IEEE Energy Conversion Congress and Exposition (ECCE)*. Nashville, US: IEEE, (To be published).

[17] N. Baker, M. Liserre, L. Dupont, and Y. Avenas, "Improved reliability of power modules: a review of online junction temperature measurement methods," *IEEE Ind. Electron. Mag.*, vol. 8, no. 3, pp. 17–27, Sep. 2014.

[18] Y. Peng, Q. Wang, H. Wang, and H. Wang, "An on-line calibration method for tsep-based junction temperature estimation," *IEEE Trans. Ind. Electron.*, vol. 69, no. 12, pp. 13 616–13 624, Dec. 2022.

[19] S. Zhao, Y. Peng, F. Yang, E. Ugur, B. Akin, and H. Wang, "Health state estimation and remaining useful life prediction of power devices subject to noisy and aperiodic condition monitoring," *IEEE Trans. Instrum. Meas.*, vol. 70, pp. 1–16, 2021.

[20] Y. Peng, S. Zhao, and H. Wang, "A digital twin based estimation method for health indicators of dc–dc converters," *IEEE Trans. Power Electron.*, vol. 36, no. 2, pp. 2105–2118, Feb. 2021.

[21] B. Gao, F. Yang, M. Chen, L. Ran, I. Ullah, S. Xu, and P. Mawby, "A temperature gradient-based potential defects identification method for igbt module," *IEEE Trans. Power Electron.*, vol. 32, no. 3, pp. 2227–2242, Mar. 2017.
[22] H. Ren, L. Ran, X. Liu, L. Liu, S. Djurovic, H. Jiang, M. Barnes, and P. A. Mawby, "Quasi-distributed temperature detection of press-pack igbt power module using fbg sensing," *IEEE J. Emerg. Sel. Topics Power Electron.*, vol. 10, no. 5, pp. 4981–4992, Oct. 2022.
[23] A. S. Bahman, K. Ma, and F. Blaabjerg, "A lumped thermal model including thermal coupling and thermal boundary conditions for high-power igbt modules," *IEEE Trans. Power Electron.*, vol. 33, no. 3, pp. 2518–2530, Mar. 2018.
[24] X. Du, J. Zhang, S. Zheng, and H.-M. Tai, "Thermal network parameter estimation using cooling curve of igbt module," *IEEE Trans. Power Electron.*, vol. 34, no. 8, pp. 7957–7971, Aug. 2019.
[25] B. Rannestad, A. E. Maarbjerg, K. Frederiksen, S. Munk-Nielsen, and K. Gadgaard, "Converter monitoring unit for retrofit of wind power converters," *IEEE Trans. Power Electron.*, vol. 33, no. 5, pp. 4342–4351, May 2018.
[26] Y. Peng, K. Chu, S. Mu, H. Cao, and H. Wang, "Parasitic effect compensation method for igbt on-state voltage measurement in traction inverter application," *IEEE Trans. Power Electron.*, vol. 37, no. 5, pp. 4937–4941, May 2022.
[27] ECPE, "ECPE guideline AQG 324 qualification of power modules for use in power electronics converter units in motor vehicles," *ECPE*, 2019.
[28] B. Rannestad, K. Fischer, P. Nielsen, K. Gadgaard, and S. Munk-Nielsen, "Virtual temperature detection of semiconductors in a megawatt field converter," *IEEE Trans. Ind. Electron.*, vol. 67, no. 2, pp. 1305–1315, Feb. 2020.
[29] J. Reimers, L. Dorn-Gomba, C. Mak, and A. Emadi, "Automotive traction inverters: current status and future trends," *IEEE Trans. Veh. Technol.*, vol. 68, no. 4, pp. 3337–3350, Apr. 2019.
[30] X. Wei, Y. Peng, B. Yao, and H. Wang, "Dc-link capacitance estimation based on discharge profile of inverter for ev application," in *2023 International Power Electronics Conference (IPEC 2023- ECCE Asia)*. Jeju, Korea: IEEE, May 2023.
[31] K. Ma, N. He, M. Liserre, and F. Blaabjerg, "Frequency-domain thermal modeling and characterization of power semiconductor devices," *IEEE Trans. Power Electron.*, vol. 31, no. 10, pp. 7183–7193, Oct. 2016.
[32] "IGBT module FS820R08A6P2B," Infineon, Tech. Rep. [Online]. Available: https://www.infineon.com/dgdl/Infineon-FS820R08A6P2B-DataSheet-v03_01-EN.pdf?fileId=5546d4625fe36784015fe7bf8e872948
[33] "Using the NTC inside a power electronic module," Infineon, Tech. Rep. [Online]. Available: https://www.infineon.com/dgdl/Infineon-AN2009_10_Using_the_NTC-ApplicationNotes-v01_00-EN.pdf?fileId=db3a304325afd6e0012628b593e62233
[34] "Film capacitor PK16," Electronicon, Tech. Rep. [Online]. Available: https://www.electronicon.com/produkte/dc-kondensatoren/pk16
[35] "IGBT module FS35R12KT3," Infineon, Tech. Rep. [Online]. Available: https://www.infineon.com/dgdl/Infineon-FS35R12KT3-DataSheet-v02_01-EN.pdf?fileId=db3a304412b407950112b431421f53f3
[36] Y. Peng and H. Wang, "A simplified on-state voltage measurement circuit for power semiconductor devices," *IEEE Trans. Ind. Electron.*, vol. 36, no. 10, pp. 10 993–10 997, Oct. 2021.
[37] "Fiber optic temperature sensor OTG-F," Opsens Solutions, Tech. Rep. [Online]. Available: https://opsens-solutions.com/products/fiber-optic-temperature-sensors/otg-f/
[38] "Universal signal converter WAS6 TTA," Weidmuller, Tech. Rep. [Online]. Available: https://catalog.weidmueller.com/catalog/Start.do?localeId=en&ObjectID=8964310000

Xing Wei (Student Member, IEEE) received the B.E. degree in electrical engineering and automation from the Nanjing Normal University, Nanjing, China, in 2016, and the M.E. degree in electrical engineering from Southeast University, Nanjing, in 2019. From September 2017 to October 2018, he was a Visiting Student with RWTH Aachen University, Aachen, Germany.

He is currently working toward the Ph.D. degree in power electronic with Aalborg University, Aalborg, Denmark, and he is a research assistant at Southeast University, Nanjing, China. His research interests include health and condition monitoring of traction inverters for electric vehicles.

Long Jin received the master's degree in automation and the Ph.D. degree in vibration, concussion, and noises from the Nanjing University of Aeronautics and Astronautics, Nanjing, China, in 1993 and 1997, respectively.

He is currently a Professor with the School of Electrical Engineering, Southeast University, Nanjing, China. His current research interests include the design and control of high-power electronics, robotics, and ultrasonic motors.

Bo Yao (Student Member, IEEE) received the B.Eng. and M.Eng. degrees in electrical engineering from Southwest Jiaotong University (SWJTU), Chengdu, China, in 2017 and 2020, respectively. He received the Ph.D. degree in power electronic with Aalborg University, Aalborg, Denmark in 2023. In 2023, he was seconded as a visiting scholar to the AAB Corporate Research Center, Vasteras, Sweden.

He is currently a Research Assistant at the Energy Department of Aalborg University. He is also a member of X-Power test facility of Aalborg University. His research interests include reliability testing, lifetime evaluation and condition monitoring of power electronic components in power converter systems.

Dr. Yao was a recipient of the Best Paper Award of International Conference on Electrical Machines and Systems (ICEMS) in 2019, and the SEMIKRON Young Engineer Award from the ECPE European Center for Power Electronics and SEMIKRON Foundation in 2023.

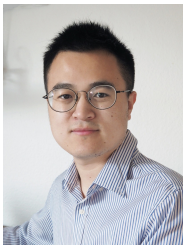

Yingzhou Peng (S'17-M'20) received the B.S. degree in electrical engineering from Harbin Engineering University, Harbin, China, in 2014, the M.S. degree in power electronics from Chongqing University, Chongqing, China, in 2017, and the Ph.D. degree in power electronics from Aalborg University, Aalborg, Denmark in 2020. From 2020 to 2022, He was a PosDoc with Aalborg University, Aalborg, Denmark.

He was a Visiting Researcher with the Electrical Power and Energy Conversion Lab, Cambridge University, Cambridge, U.K, in 2020. He is currently working as an Assistant Professor at Hunan Unversity, China.

His research interests include the failure mechanisms analysis of power electronic components, the improvement of the robustness and reliability of power converters by means of condition monitoring.

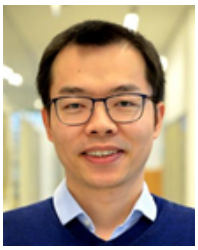

Huai Wang (Senior Member, IEEE) received the B.E. degree in electrical engineering from the Huazhong University of Science and Technology, Wuhan, China, in 2007, and the Ph.D. degree in power electronics from the City University of Hong Kong, Hong Kong, in 2012.

He is currently a Professor with AAU Energy, Aalborg University, Aalborg, Denmark, where he leads the Group of Reliability of Power Electronic Converters (ReliaPEC) and the mission on Digital Transformation and AI. He was a Visiting Scientist with ETH Zurich, Switzerland, from August to September 2014, and with the Massachusetts Institute of Technology, Cambridge, MA, USA, from September to November 2013. He was with the ABB Corporate Research Center, Switzerland in 2009. His research interests include the fundamental challenges in modeling and validation of power electronic component failure mechanisms and application issues in system-level predictability, condition monitoring, circuit architecture, and robustness design.

Dr. Wang was the recipient of the Richard M. Bass Outstanding Young Power Electronics Engineer Award from the IEEE Power Electronics Society, in 2016, and the 1st Prize Paper Award from IEEE TRANSACTIONS ON POWER ELECTRONICS, in 2021. He serves as an Associate Editor for the Journal of Emerging and Selected Topics in Power Electronics and IEEE TRANSACTIONS ON POWER ELECTRONICS.